

Article

**A Hexagonal Prismatic Porphyrin Array: Synthesis, STM
Detection, and Efficient Energy Hopping in Near-Infrared Region**

Min-Chul Yoon, Zin Seok Yoon, Sung Cho, and Dongho Kim
Akihiko Takagi, Takuya Matsumoto, and Tomoji Kawai
Takaaki Hori, Xiaobin Peng, Naoki Aratani, and Atsuhiko Osuka

J. Phys. Chem. A, **2007**, 111 (38), 9233-9239 • DOI: 10.1021/jp0723923

Downloaded from <http://pubs.acs.org> on December 29, 2008

More About This Article

Additional resources and features associated with this article are available within the HTML version:

- Supporting Information
- Access to high resolution figures
- Links to articles and content related to this article
- Copyright permission to reproduce figures and/or text from this article

[View the Full Text HTML](#)



ACS Publications
High quality. High impact.

A Hexagonal Prismatic Porphyrin Array: Synthesis, STM Detection, and Efficient Energy Hopping in Near-Infrared Region[†]

Min-Chul Yoon, Zin Seok Yoon, Sung Cho, and Dongho Kim*

Department of Chemistry, Yonsei University, Seoul 120-749, Korea

Akihiko Takagi, Takuya Matsumoto, and Tomoji Kawai

Core Research for Evolutional Science and Technology (CREST), Japan Science and Technology Agency (JST), The Institute of Scientific and Industrial Research (ISIR), Osaka University, 8-1, Mihogaoka, Ibaragi, Osaka 567-0047, Japan

Takaaki Hori, Xiaobin Peng, Naoki Aratani, and Atsuhiko Osuka*

Department of Chemistry, Graduate School of Science, Kyoto University, Sakyo-ku, Kyoto 606-8502, Japan

Received: March 27, 2007; In Final Form: May 15, 2007

A belt-shaped hexagonal cyclic porphyrin array **2** that comprises of six *meso*–*meso*, β – β , β – β triply linked diporphyrins **3** bridged by 1,3-phenylene spacers is prepared by oxidation from cyclic dodecameric array **1** consisting of six *meso*–*meso* directly linked diporphyrins **4** with DDQ and Sc(OTf)₃. The absorption spectrum of **2** is similar to that of the constituent subunit **3** but shows a slight red-shift for the Q-bands in near-infrared (NIR) region, indicating the exciton coupling between the neighboring diporphyrin chromophores. Observed total exciton coupling energies in the absorption spectra were largely matched with the calculated values based on point-dipole exciton coupling approximation. It was found that the experimental exciton coupling strength (292 cm⁻¹) of the Q-band in **2** is slightly larger than the calculated one (99 cm⁻¹), indicating that the electronic communications are enhanced through 1,3-phenylene linkers in hexameric macromolecule. A rate of the excitation energy hopping (EEH) that occurs in **2** at the lowest excited singlet state in the near-infrared region has been determined to be (1.8 ps)⁻¹ on the basis of the pump-power dependent femtosecond transient absorption (TA) and the transient absorption anisotropy (TAA) decay measurements. The 2 times faster EEH rate of **2** than that of **1** (4.0 ps)⁻¹ mainly comes from involving through-bond energy transfer among diporphyrin subunits via 1,3-phenylene bridges as well as Förster-type through-space EEH processes. STM measurement of **2** in the Cu(100) surface revealed that it takes several discrete conformations with respect to the relative orientation of neighboring diporphyrins. Collectively, an effective EEH in the NIR region is realized in **2** due largely to the intensified oscillator strength in the S₁ state (Q-band) and the close proximity held by 1,3-phenylene spacers.

Introduction

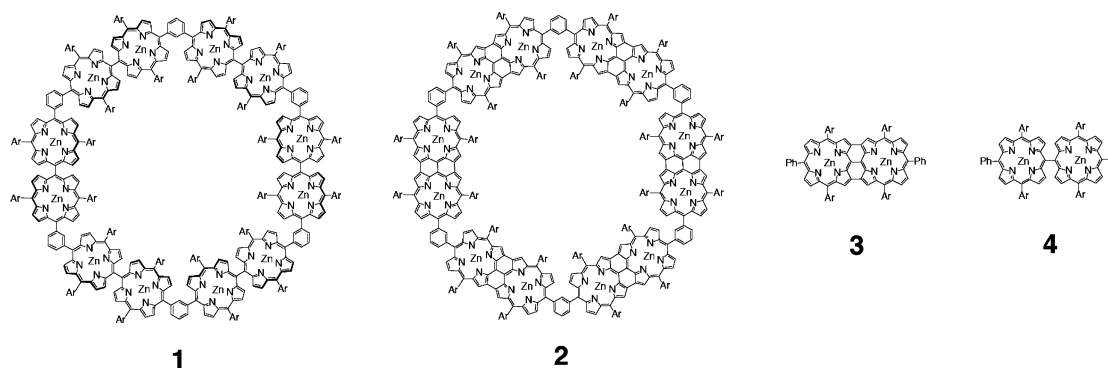
Inspired by the wheel-like architectures of photosynthetic pigments (LH1 and LH2),¹ covalently or noncovalently linked cyclic porphyrin arrays have been extensively explored as artificial light-harvesting antenna models.^{2–4} Despite these efforts, the realization of high efficiency in excitation energy transfer (EET) still remains a challenge, particularly for the process that can operate in the near-infrared (NIR) region. NIR-EET is highly promising in light of emerging optoelectronic materials functioning at long wavelength (1.2–1.5 μ m) irradiation, because it enables the communication between different functional units, the modulation of efficiency, and the sensing of important species when linked to a reporter chromophore.⁵ However, such NIR-EET is usually quite difficult because of intrinsic short lifetimes of such NIR excited states and a lack of strong absorption in NIR region. Excited states whose excitation energy is lying in the NIR region are often short-lived due to accelerated nonradiative decay to the ground state, which arises from large Franck–Condon factor. To realize such

NIR energy transfer, chromophores with strong NIR absorption have to be closely held in a well-defined manner.

In the past decade, we have explored various porphyrin arrays on the basis of the Ag(I)-promoted *meso*–*meso* coupling reaction of 5,15-diaryl Zn(II) porphyrins,⁶ which includes 3D-extending windmill arrays,^{7a,b} extremely long arrays,^{7c,d} and cyclic arrays.⁴ The excited-state dynamics of these porphyrin arrays have been extensively studied by short pulse laser-based spectroscopies, which revealed efficient excitation energy hopping along the arrays.⁸ In addition, these *meso*–*meso* linked porphyrin arrays become to display large two-photon absorption cross sections as intriguing attributes, when the conjugative electronic interactions along the arrays are increased by the dihedral angle control.⁹ As an extension of these studies, *meso*–*meso*, β – β , β – β triply linked diporphyrins were prepared as fully conjugated chromophores and their excited-state dynamics and nonlinear optical properties were reported, in which the elongation of π -conjugation lengths provided NIR-extended absorption and emission up to 3 μ m for triply fused dodecamer.^{10,11} Despite the promising electronic properties of these triply linked porphyrin arrays, there is only a limited number of examples that include the triply linked porphyrin arrays as a part of sophisticated large molecular systems.^{11,12}

[†] Part of the “Sheng Hsien Lin Festschrift”.

* Corresponding authors. E-mail: D.K., dongho@yonsei.ac.kr; A.O., osuka@kuchem.kyoto-u.ac.jp.

CHART 1: Molecular Structures of This Paper (Ar = *p*-Dodecyloxyphenyl)

In this paper, we report the synthesis of a hexagonal cyclic array **2** that consists of six *meso-meso*, $\beta-\beta$, $\beta-\beta$ triply linked diporphyrins **3** bridged by 1,3-phenylene spacers (Chart 1). Efficient excitation energy hopping (EEH) dynamics in the lowest excited state that can operate in the NIR region are studied by the femtosecond transient absorption (TA) and the transient absorption anisotropy (TAA) decay measurements. Furthermore, conformational information can be analyzed by adsorption behaviors of **2** on the metal surface using the STM measurement.

Experimental Methods

General Procedures. All reagents and solvents were of the commercial reagent grade and were used without further purification except where noted. Dry toluene was obtained by distilling over CaH₂. ¹H NMR spectra were recorded on a JEOL delta-600 spectrometer, and chemical shifts were reported as the δ scale in ppm relative to CH₂Cl₂ (δ 5.32 ppm). The spectroscopic grade THF was used as solvents for all spectroscopic studies. UV/visible absorption spectra were recorded on a Shimadzu UV-3150 spectrometer. Mass spectra were recorded on a Shimadzu/KRATOS KOMPACT MALDI 4 spectrometer, using positive-MALDI ionization method with dithranol matrix.

Hexagonal Cyclic Array 2. The cyclic dodecameric array **1** prepared as light-harvesting antenna model^{4a} was oxidized with 36 equiv of 2,3-dichloro-5,6-dicyano-1,4-benzoquinone (DDQ, 4 mg, 16 μ mol) and Sc(OTf)₃ (8 mg, 16 μ mol) in toluene at 110 °C for 1.5 h under dry N₂ and subsequent separation through a short alumina column provided **2** as black solids in 75% yield (3.0 mg). UV/vis: λ_{max} (THF)/nm 424 ($\epsilon/\text{dm}^3 \text{ mol}^{-1} \text{ cm}^{-1}$ 526000), 482 (267000), 568 (457000), 593 (502000), 1003 (78500), and 1144 nm (120000). Although the ¹H NMR spectrum of **2** was too broad to record signals in most of the solvents probably because of extensive aggregation, the molecular parent ion peak was detected at $m/z = 11146$ (calcd for C₇₀₈H₇₉₂N₄₈O₂₄Zn₁₂, 11143) by using MALDI-TOF MS, and the absorption spectrum of **2** is essentially the same as that of triply linked diporphyrin **3** with slight red shift, indicating that all the *meso-meso* linked diporphyrins were converted into the triply linked diporphyrins.

Meso-meso, $\beta-\beta$, $\beta-\beta$ Triply Linked Zn(II) Diporphyrin 3. *Meso-meso* linked diporphyrin **4** (20 mg, 0.010 mmol) was oxidized with DDQ (14 mg, 0.060 mmol) and Sc(OTf)₃ (31 mg, 0.060 mmol) in toluene at 110 °C for 1.5 h under N₂. The mixture was passed directly through an alumina column and evaporated. The yield of **3** was 63% (13 mg). UV/vis: λ_{max} (THF)/nm 421 ($\epsilon/\text{dm}^3 \text{ mol}^{-1} \text{ cm}^{-1}$ 144000), 469 (60800), 564 (121000), 580 (118000), 960 (17600), and 1107 nm (35100). ¹H NMR (600 MHz; CD₂Cl₂): δ 7.73–7.71 (4H, m, phenyl-

H), 7.60 (8H, d, $J = 8.2$ Hz, Ar-H), 7.53–7.51 (10H, m (6H, phenyl-H; 4H, *por-\beta*)), 7.49 (4H, d, $J = 4.6$ Hz, *por-\beta*), 7.02 (8H, d, $J = 8.2$ Hz, Ar-H), 7.01 (s, 4H, *por-\beta*), 4.10 (8H, t, $J = 6.4$ Hz, dodecyloxy), 1.88–1.85 (8H, m, dodecyloxy), 1.58–1.54 (8H, m, dodecyloxy) 1.49–1.45 (8H, m, dodecyloxy), 1.42–1.25 (56H, m, dodecyloxy), and 0.91 (12H, t, $J = 6.9$ Hz, dodecyloxy). MALDI-TOF MS found m/z 1929, calcd for C₁₂₄H₁₃₈N₈O₄Zn₂, m/z 1935.

STM Measurements. Clean flat Cu(100) surfaces were obtained by Ar⁺ sputtering and annealing (580 °C) cycles for a substrate. The porphyrin ring molecules dissolved into CHCl₃ were deposited by spraying a ca. 0.5 μ L of the solution onto the substrate in vacuum (10^{-6} mbar) using a pulse injection method, which is suited for deposition of large fragile molecules with escaping decomposition often encountered in sample deposition from the gas phase. In-situ STM measurements were performed at room temperature in ultrahigh vacuum ($<10^{-10}$ mbar) with a homebuilt STM by using an electrochemical etched Pt/Ir tip. STM image was obtained in constant current mode.

Femtosecond Transient Absorption Spectroscopy. The dual-beam femtosecond time-resolved transient absorption spectrometer consisted of a self-mode-locked femtosecond Ti:sapphire oscillator (Coherent, MIRA), a Ti:sapphire regenerative amplifier (Clark MXR model TRA-1000) that was pumped by a Q-switched Nd:YAG laser (Clark MXR model ORC-1000), a pulse stretcher/compressor, an optical parametric amplifier (Clark MXR model IR-OPA), and an optical detection system. A femtosecond Ti:sapphire oscillator pumped by a continuous wave (cw) Nd:YVO₄ laser (Coherent, Verdi) produces a train of ~ 80 fs mode-locked pulses with an averaged power of 650 mW at 800 nm. The amplified output beam regenerated by chirped pulse amplification (CPA) had a pulse width of ca. 150 fs and a power of ca. 1 W at a repetition rate of 1 kHz, which was divided into two parts by a 1:1 beam splitter. One part was color-tuned for the pump beam by an optical parametric generation and amplification (OPG-OPA). The resulting laser pulse had a temporal width of ~ 150 fs in the vis/NIR range. The pump beam was focused to a spot diameter of ~ 1 mm, and the laser fluence was adjusted, using a variable neutral-density filter. The other part was focused onto a flowing water cell to generate a white-light continuum, which was again split into two parts. One part of the white-light continuum was overlapped with the pump beam at the sample to probe the transient, and the other part of the white-light continuum was passed through the sample without overlapping the pump beam. The time delay between pump and probe beams was controlled by making the pump beam travel along a variable optical delay line. The white-light continuum beams after the sample were sent through an appropriate interference filter and then were

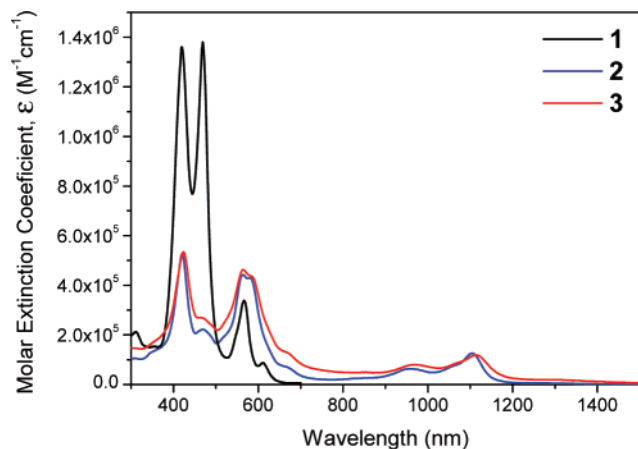


Figure 1. UV/vis absorption spectra of **1–3** in THF. That of **3** is normalized to **2** at the Soret band.

TABLE 1: Band Maxima and Molar Extinction Coefficients in the Steady-State Absorption Spectra of 2 and 3

sample	absorption/nm (molar extinction coefficient/M ⁻¹ cm ⁻¹)			
	Soret (high)	Soret (low)	Q(1,0)	Q(0,0)
2	424 (526000)	568 (457000)	1003 (78500)	1144 (120000)
3	421 (144000)	564 (121000)	960 (17600)	1107 (35100)

detected by two photodiodes. The outputs from the two photodiodes at the selected wavelength were processed by a combination of a boxcar averager and a lock-in amplifier, to calculate the absorption difference at the desired time delay between pump and probe pulses. The angle between pump and probe was set to the magic angle (54.7°). For time-resolved TAA measurement, both $I_{||}$ and I_{\perp} signals were collected individually using a thin half-wave plate with a Glan-laser polarizer.

$$r(t) = (I_{||} - I_{\perp}) / (I_{||} + 2I_{\perp})$$

where $I_{||}$ and I_{\perp} represent TA signals with the polarizations of the pump and probe pulses being mutually parallel and perpendicular, respectively. For all TA and TAA measurements, a thin absorption cell (1 mm path length) was used.

Results and Discussion

Absorption Spectra and Exciton Coupling Strength. Figure 1 shows the steady-state absorption spectra of **1**, **2** and **3** in THF solvent. The overall features in the absorption spectra of **1** are similar to those of **4** except for peak positions due to exciton coupling among neighboring porphyrin dimer units, which can be well described by the exciton coupling model.^{4,7,8,13} Interestingly, the absorption spectrum of **3** is different from those of **1** and **4** in which the absorption bands are much broader than those of orthogonal arrays and widely distributed from UV to NIR region mainly due to delocalization of π -electrons within the whole molecular framework.^{10d,11} Three distinct bands corresponding to S_2 , S_2' , and S_1 electronic transitions of **3** appear at around 421, 564, and 1107 nm, which are denoted as band I, II, and III, respectively and the electronic nature of these bands is similar to that in directly linked porphyrin dimer **4**.^{10d} Hence, the bands I, II, and III are denoted as Soret (or B-band), low-energy Soret, and Q-band, respectively, for compounds **2** and **3** (Table 1). Hexameric wheel-like molecule **1** shows exciton coupling interaction among constituent units **4** over 1,3-phenylene linkage giving rise to (1) increased splitting of the Soret band, (2) increased intensity of the Q-bands, and (3) red shift of the Q-bands.¹³ On the other hand, additional exciton

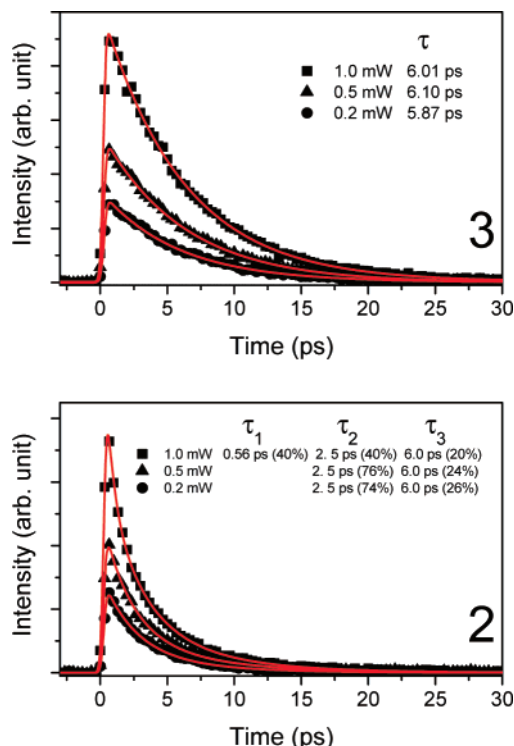


Figure 2. Pump-power dependent TA decay profiles of **3** (top) and **2** (bottom). The pump powers used are inserted. The pump and probe wavelengths were 1144 and 570 nm, respectively. The decay time constants of τ_2 and τ_3 were fixed to be 2.5 and 6 ps, respectively, in the fitting procedure of compound **2**.

coupling of B-band in **2** is not so significant as compared with its constituent unit **3**. Thus, a slight red shift in Q-bands of **2** indicates that electronic coupling induced by enhanced π -conjugation through 1,3-phenylene linkage occurs in **2** due to elongation of π -conjugation pathway within constituent unit **3**.

The exciton coupling energy $\Delta V_{\text{cal}}(\text{B})$ and $\Delta V_{\text{cal}}(\text{Q})$ based on point dipole coupling approximation can be calculated to analyze the absorption maximum positions of constituent unit **3** and cyclic wheel **2** (see Supporting Information).^{14,15} The total exciton coupling energy $\Delta V_{\text{cal}}(\text{B})$ for the B-band in **2** is calculated to be 795 cm⁻¹. According to the absorption spectra, the experimental exciton coupling energy $\Delta V_{\text{exp}}(\text{B})$ in **2** is determined to be 125 cm⁻¹. There is a large discrepancy in exciton coupling energy especially for the B-band, which is mainly caused by a difficulty in evaluating the exact experimental value due to the spectral congestion with many charge-transfer bands in Soret band region.^{10d} Furthermore, as compared to **3**, broad absorption peaks in Soret region of **2** are observed presumably through H- and J-type couplings among the six subunits **3**, which gives rise to complicated exciton coupling phenomena. In a similar manner, the total exciton coupling energy $\Delta V_{\text{cal}}(\text{Q})$ for the Q-band in the NIR region can be estimated to be 99 cm⁻¹, which is somewhat smaller than the experimental value of 292 cm⁻¹. This discrepancy can be described by a red shift in the Q-band of **2** contributed by the enhancement of π -delocalization within hexameric cyclic macromolecule. Overall, it is inferred that B-bands corresponding to the electronically allowed transition have larger transition dipole moments leading to Förster-type through-space excitonic coupling. In Q-bands of **2**, on the other hand, the elongation of the π -conjugation pathway is more sensitive to the Dexter-type through-bond effect because the Q-band is originated from out-of-phase configuration interactions between HOMO–LUMO transitions of porphyrin macrocycle.

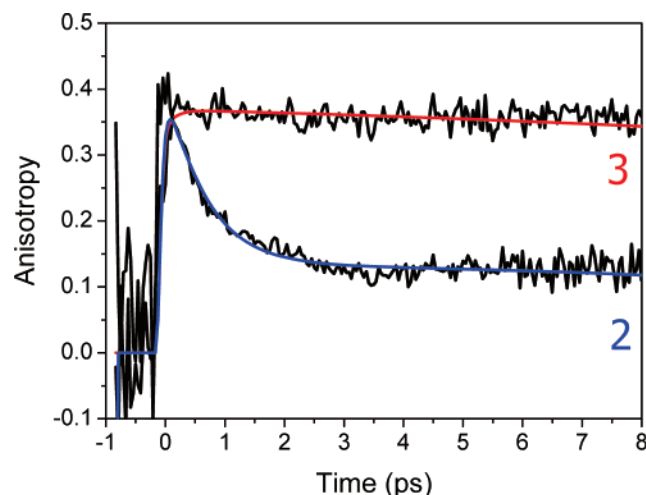


Figure 3. Temporal profiles of transient absorption anisotropy decays (black lines) of **3** and **2**. The pump and probe wavelengths were 1144 and 570 nm, respectively.

Transient Absorption and Excitation Energy Hopping. To reveal the fast EEH processes occurring in **2**, femtosecond transient absorption measurement was employed where ground-state bleaching recovery signals in the low-energy B state (570 nm) were recorded with Q-band excitation (1144 nm) to eliminate the involvement of S_2 – S_1 internal conversion for all molecular systems (Figure 2). With the pump power dependence on the TA signal, we were able to clarify the EEH process in **2**. Although **3** reveals no power dependence on the TA decay with only slow decay component in agreement with the S_1 -state lifetime observed in our previous work (6.0 ps for **3**),^{10d} the TA decay of **2** is sensitive to the pump power, indicating S_1 – S_1 exciton–exciton annihilation processes because the intense irradiation may generate two or more excitons in one cyclic array system, and then, the recombination between excitons gives rise to a fast deactivation channel. Hence, the initial fast decay component (2.5 ps) in **2** can be assigned as exciton–exciton annihilation times in the S_1 state because the exciton–exciton annihilation is the migration-limited process. In addition, high order exciton–exciton annihilation processes with a time constant of ~ 560 fs were observed at photoexcitation intensity of 1 mW in the case of compound **2**. It is generally accepted that as the number of chromophores increases, there would be an increasing chance for the presence of high order multiple exciton–exciton annihilation processes in multichromophoric system, which provides multicomponents in the TA signal as seen in the previous study for compound **1**.^{13,14}

Figure 3 shows the femtosecond TA anisotropy decays of hexameric wheel **2** along with its corresponding subunit **3** in THF with the same pump–probe wavelengths used in TA measurement. Only single TAA decay component with $\tau = \sim 400$ ps was detected, which has been assigned to rotational diffusion time in **3**. In **2**, on the other hand, another fast decay component with $\tau = 0.63$ ps was observed in addition to slow rotational diffusion time (> 5 ns). In **2**, because rotational diffusion times are much longer than these time constants due to their large molecular volumes, the observed depolarization times should be associated with the excitation energy hopping processes. Because there is no fast decay component within 8 ps range in **3**, triply linked **3** cannot be regarded as dichromophoric system composed of two Zn(II) porphyrin moieties. Thus, a single-exponential decay time constant of 630 fs in **2** can be adequately assigned to its EEH time along the ring.

To reveal the relationship between anisotropy decay and excitation energy hopping rate, a simple theoretical model can be introduced (Scheme 1). In this model, the main assumptions are that the intermolecular interactions are very weak and the EEH processes occur only between the adjacent porphyrin subunits **3**. When porphyrin unit is photoexcited, the time evolution of excitation energy population in each chromophore in cyclic hexamer can be described by master eq 1 composed of a series of differential rate equations.¹⁶

$$\frac{d\mathbf{P}}{dt} = \mathbf{K}\mathbf{P} \quad (1)$$

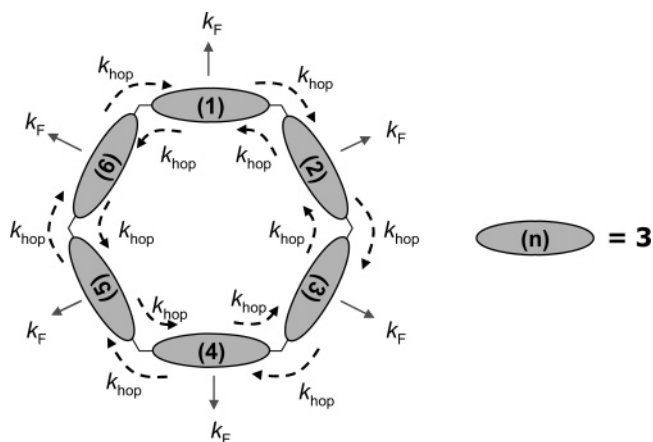
where \mathbf{P} is the excitation energy population vector and \mathbf{K} is the rate coefficient. For the hexameric wheel, \mathbf{K} is expressed by a 6×6 matrix.

$$\mathbf{K} = \begin{bmatrix} -(k_F + 2k_{\text{hop}}) & k_{\text{hop}} & 0 & 0 & 0 & k_{\text{hop}} \\ k_{\text{hop}} & -(k_F + 2k_{\text{hop}}) & k_{\text{hop}} & 0 & 0 & 0 \\ 0 & k_{\text{hop}} & -(k_F + 2k_{\text{hop}}) & k_{\text{hop}} & 0 & 0 \\ 0 & 0 & k_{\text{hop}} & -(k_F + 2k_{\text{hop}}) & k_{\text{hop}} & 0 \\ 0 & 0 & 0 & k_{\text{hop}} & -(k_F + 2k_{\text{hop}}) & k_{\text{hop}} \\ k_{\text{hop}} & 0 & 0 & 0 & k_{\text{hop}} & -(k_F + 2k_{\text{hop}}) \end{bmatrix} \quad (2)$$

where k_F and k_{hop} represent the fluorescence decay and hopping rates, respectively. Because our porphyrin array systems have well-ordered transition dipole moments, the anisotropy decay $r(t)$ can be described by following equations from the diagonalization of matrix \mathbf{K} (see Supporting Information),¹⁷

$$r(t) = 0.1 + 0.3 \exp(-3k_{\text{hop}}t) \quad (3)$$

SCHEME 1: Schematic Diagram of Excitation Energy Migration and Relaxation Pathways in 2



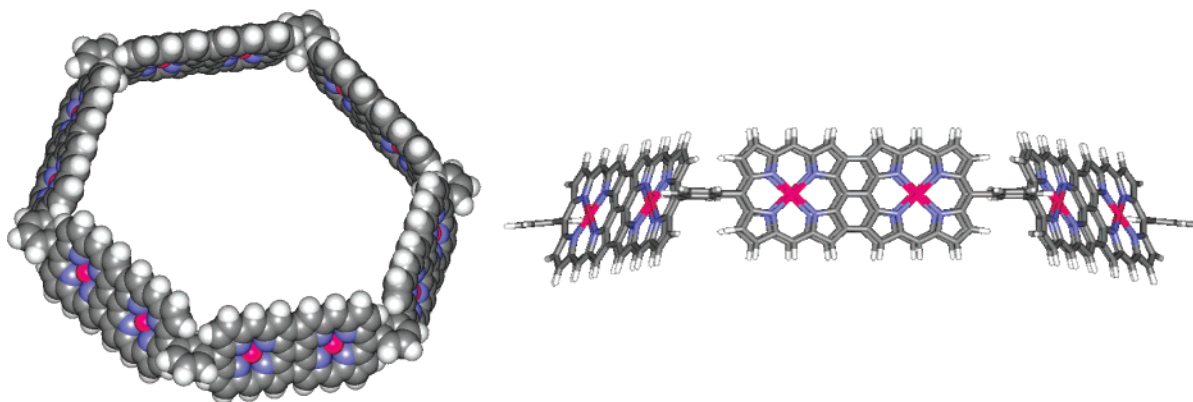


Figure 4. Three-dimensional geometries of **2** optimized at semiempirical PM3 level.

According to eq 3, the anisotropy decay rate k_{dep} for all cyclic hexamers is 3 times larger than excitation energy hopping rate k_{hop} :

$$k_{\text{dep}} = 3k_{\text{hop}} \quad \text{and} \quad 3\tau_{\text{dep}} = \tau_{\text{hop}} \quad (4)$$

for the hexameric wheel system. The identical relationship between depolarization and hopping rates can be also obtained in different ways (*vide infra*).

The observed anisotropy decay and exciton–exciton annihilation phenomena of the cyclic hexamer can be fully described by the Förster-type incoherent energy hopping model.¹⁸ The EEH time for cyclic arrays is strongly correlated with the depolarization time τ_{dep} as well as the exciton–exciton annihilation time τ_{annihil} as follows (eqs 5 and 6).

$$\tau_{\text{dep}} = \frac{\tau_{\text{hop}}}{4[1 - \cos^2(2\pi/N)]} = \frac{\tau_{\text{hop}}}{4(1 - \cos^2 \alpha)} \quad (5)$$

$$\tau_{\text{annihil}} = \frac{N^2 - 1}{24} \tau_{\text{hop}} \quad (6)$$

where N is the number of hopping sites and α is the angle between the neighboring transition dipole moments. Because it is relevant to assume that subunit **3** acts as a single chromophore for cyclic hexamers **2**, N equals 6 ($\alpha = 60^\circ$). Consequently, for compound **2**, eqs 5 and 6 can be simplified as $\tau_{\text{hop}} = 3\tau_{\text{dep}}$ and $\tau_{\text{hop}} = 0.686\tau_{\text{annihil}}$, in which the former equation is exactly the same as the consequence by matrix diagonalization of \mathbf{K} (eq 4). The excitation energy hopping time can be obtained to be 1.89 ps by eqs 4 and 5, and also, calculated to be 1.72 ps by eq 6; hence, the EEH time from the arithmetically averaged value from two methods is 1.8 ps for **2**. Although **1** and **2** have similar structural parameters such as interchromophoric distances and angles, etc., the EEH time of **2** is 2 times faster than that of **1** (4.0 ps) indicating that Dexter-type through-bond EET processes via 1,3-phenylene linkage are involved in the case of **2**.¹³ This result is in good accordance with a slight but distinct red shift of Q-band mainly due to the enhancement of π -conjugation via 1,3-phenylene linkage as seen in the absorption spectra of **2** (Figure 1). On the contrary, the EEH time of a cyclic hexameric system (36 ps) consisting of six *meso*–*meso* directly linked Zn(II) porphyrin tetramer becomes 9 times slower than that of **1**, which is mainly due to weak exciton coupling caused by increasing interchromophoric distance between their constituent Zn(II) porphyrin tetramer units.^{4c}

Structure and STM Detection. According to quantum mechanical calculation at the PM3 level, the optimized structure of **2** is highly symmetric hexagonal from a top view and

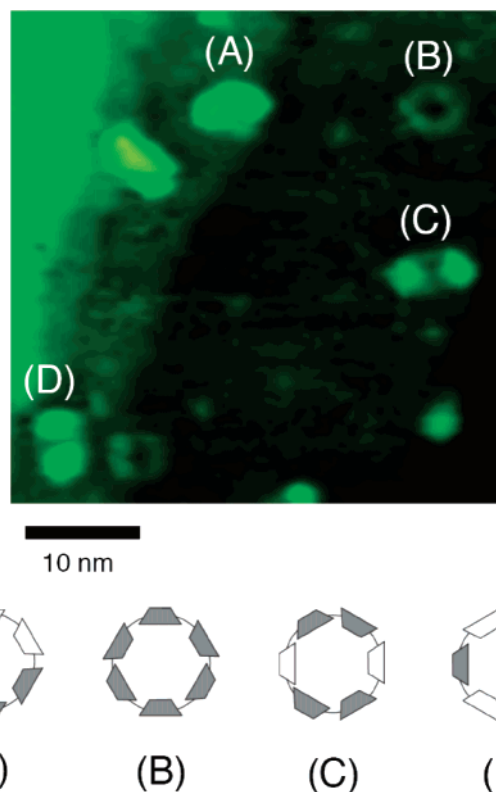


Figure 5. STM images of **2** on Cu(100). (A)–(D) are representative conformations.

trapezoidal shape from a side view (Figure 4). Average dihedral angle between neighboring phenylene linker and monomeric unit **3** lies in the range 67 – 75° , which enables electronic interaction between them. Hence, moderately decreased dihedral angle could delocalize π -electrons more efficiently to entire cyclic macromolecule, which can lead to Dexter-type through-bond energy transfer processes in **2**. Moreover, well-defined structure and enhanced rigidity by triply linking of **3** can accelerate energy migration processes in **2**.

To confirm the structure of **2**, the scanning tunneling microscopy (STM) detection has been attempted. A dilute solution of **2** in CHCl_3 was sprayed in vacuum (10^{-6} mbar) using a pulse injection method onto a clean flat Cu(100) surface that was obtained by repeated cycles of annealing and Ar-ion sputtering.^{19,20} In situ STM measurements were performed at room temperature with a home-built STM using an electrochemical etched Pt/Ir tip under ultrahigh vacuum ($<10^{-10}$ mbar) in a constant current mode. Under these conditions, **1** exhibits ring spots with an average diameter of 3.5 ± 0.67 nm and an

average height of 0.29 ± 0.12 nm, most of which are regular in shape and size,^{4a} suggesting its relatively homogeneous adsorption and conformation on the surface. The homogeneous STM images are probably arising from the relatively weak interactions due to the orthogonal conformation of *meso-meso* linked diporphyrin moieties **4**. On the other hand, the STM images of **2** taken with a sample bias (V_s) of 1.5 V and a tunneling current (I) of 15 pA display several discrete shapes with similar diameters of 3.6–3.8 nm, which are roughly in agreement with the hexagonal prismatic shape (Figure 5). This observation stems from the stronger interaction of the planar triply linked diporphyrin units with the metal surface.²¹ In the array **2**, the planar diporphyrin segments **3** are nearly perpendicular to the whole macrocyclic plane, and thus when one diporphyrin segment is adsorbed on the surface, the conformation of **2** may become distorted, varying upon the way of subsequent adsorption of diporphyrin segments, which gives rise to several conformations only with rotating diporphyrin plane with respect to macrocyclic plane. A model study indicates that the alternate conformation, where the constituent diporphyrins are bent alternately to different direction, is sterically most stable and expected to have the lowest height on the surface. Thus, spot B may correspond to this conformation, because its height is the lowest (0.24 nm) among the observed ones. Spots A, C, and D can be tentatively assigned to respective conformations shown in Figure 5 on the basis of their patterns of the imaging contrast and the heights (ca. 0.46 nm).

These STM data show the possibility for the coexistence of a few conformational isomers on metal surfaces in ultrahigh vacuum environment, strictly speaking, in which surrounding medium is not the same as in transient absorption measurement. Although conformational isomers can still exist in solution, our theoretical calculation for EEH model based on the assumption of symmetric hexagonal structures might be applicable to real nature due to the maintenance of overall hexagonal shapes in spite of inhomogeneous structures as shown in STM images.

Conclusions

We have investigated the excitation energy migration process in the S_1 state of cyclic porphyrin arrays **2** synthesized via oxidation of **1** with DDQ and $\text{Sc}(\text{OTf})_3$. The excitation energy hopping time of **2** was estimated to be 1.8 ps using both femtosecond TA anisotropy measurements and exciton–exciton annihilation processes in S_1 state. Despite the low excitation energy (ca. 1.08 eV) in the NIR region, as compared to **1**, efficient and fast excitation energy migration processes occur in **2** through a contribution of through-bond EEH processes over 1,3-phenylene linkage between the constituent subunit **3**. Furthermore, from the result of quantum mechanical calculation, structural rigidity and well-oriented hexagonal structure in **2** are illustrated, which is an important factor in the enhancement of the rate and efficiency of EEH processes. We suggest that two-dimensional cyclic arrays **2** are good candidates in view of efficient EEH processes for artificial biomimic light harvesting apparatus especially in NIR region due to their stronger electronic and excitonic coupling with a rigid circular geometry.

Acknowledgment. The work at Yonsei University was supported by the Star Faculty Program of the Ministry of Education and Human Resources Development, Korea. The work at Kyoto University was supported by a Grant-in-Aid from the Ministry of Education, Culture, Sports, Science and Technology, Japan. M.-C.Y. and S.C. acknowledge the fellowship

of the BK 21 program from the Ministry of Education and Human Resources Development. T.H. thanks the JSPS fellowship for Young Scientists.

Supporting Information Available: Calculation of exciton coupling strength and mathematical analyses of rate expressions for excitation energy hopping. This material is available free of charge via the Internet at <http://pubs.acs.org>.

References and Notes

- (1) (a) McDermott, G. M.; Prince, S. M.; Freer, A. A.; Hawthorthwaite-Lawless, A. M.; Papiz, M. Z.; Cogdell, R. J.; Isaacs, M. W. *Nature* **1995**, *374*, 517. (b) Karrasch, S.; Bullough P. A.; Ghosh, R.; *EMBO J.* **1995**, *14*, 631. (c) Koepke, J.; Hu, X.; Muenke, C.; Schulten, K.; Michel, H. *Structure* **1996**, *4*, 581. (d) McLuskey, K.; Prince, S. M.; Cogdell, R. J.; Isaacs, M. W. *Biochemistry* **2001**, *40*, 8783. (e) Roszak, A., W.; Howard, T. D.; Southall, J.; Gardiner, A. T.; Law, C. J.; Isaacs, N. W.; Cogdell, R. J. *Science* **2003**, *302*, 1969.
- (2) (a) Mongin, O.; Schuwey, A.; Vallot, M.-A.; Gossauer, A. *Tetrahedron Lett.* **1999**, *40*, 8347. (b) Anderson, S.; Anderson, H. L.; Sanders, J. K. M. *Acc. Chem. Res.* **1993**, *26*, 469. (c) Li, J.; Ambrose, A.; Yang, S. I.; Diers, J. R.; Seth, J.; Wack, C. R.; Bocian, D. F.; Hoten, D.; Lindsey, J. S. *J. Am. Chem. Soc.* **1999**, *121*, 8927. (d) Biemans, H. A. M.; Rowan, A. E.; Verhoeven, A.; Vanoppen, P.; Latterini, L.; Foekema, J.; Schenning, A. P. H. J.; Meijer, E. W.; De Schryver, F. C.; Nolte, R. J. M. *J. Am. Chem. Soc.* **1998**, *120*, 11054. (e) Sugiura, K.; Fujimoto, Y.; Sakata, Y. *Chem. Commun.* **2000**, 1105.
- (3) Noncovalent assemblies of dodecameric and nonameric porphyrin arrays were reported. (a) Takahashi, R.; Kobuke, Y. *J. Am. Chem. Soc.* **2003**, *125*, 2372. (b) Rucareanu, S.; Mongin, O.; Schuwey, A.; Hoyler, N.; Gossauer, A.; Amrein, W.; Hediger, H.-U. *J. Org. Chem.* **2001**, *66*, 4973.
- (4) (a) Peng, X.; Aratani, N.; Takagi, A.; Matsumoto, T.; Kawai, T.; Hwang, I.-W.; Ahn, T. K.; Kim, D.; Osuka, A. *J. Am. Chem. Soc.* **2004**, *126*, 4468. (b) Nakamura, Y.; Hwang, I.-W.; Aratani, N.; Ahn, T. K.; Ko, D. M.; Takagi, A.; Kawai, T.; Matsumoto, T.; Kim, D.; Osuka, A. *J. Am. Chem. Soc.* **2005**, *127*, 236. (c) Hori, T.; Aratani, N.; Takagi, A.; Matsumoto, T.; Kawai, T.; Yoon, M.-C.; Yoon, Z. S.; Cho, S.; Kim, D.; Osuka, A. *Chem. Eur. J.* **2006**, *12*, 1319.
- (5) (a) Kronick, M. N. *J. Immun. Methods* **1986**, *92*, 1. (b) Pizzoferrata, R.; Lagonigro, L.; Ziller, T.; Di, Carlo, A.; Paolesse, R.; Mandoj, F.; Rocci, A.; Lo, Sterzo, C. *Chem. Phys.* **2004**, *300*, 217. (c) Rolinski, O. J.; Birch, D. J. S.; McCartney, L. J.; Pickup, J. C. *Chem. Phys. Lett.* **1999**, *309*, 395.
- (6) (a) Osuka, A.; Shimidzu, H. *Angew. Chem., Int. Ed. Engl.* **1997**, *36*, 135. (b) Aratani, N.; Osuka, A. *Bull. Chem. Soc. Jpn.* **2001**, *74*, 1361. (c) Aratani, N.; Tsuda, A.; Osuka, A. *Synlett* **2001**, 1663.
- (7) (a) Nakano, A.; Osuka, A.; Yamazaki, I.; Yamazaki, T.; Nishimura, Y. *Angew. Chem., Int. Ed.* **1998**, *37*, 3023. (b) Nakano, A.; Yamazaki, T.; Nishimura, Y.; Yamazaki, I.; Osuka, A. *Chem. Eur. J.* **2000**, *6*, 3254. (c) Aratani, N.; Osuka, A.; Kim, Y. H.; Jeong, D. H.; Kim, D. *Angew. Chem., Int. Ed.* **2000**, *39*, 1458. (d) Aratani, N.; Takagi, A.; Yanagawa, Y.; Matsumoto, T.; Kawai, T.; Yoon, Z. S.; Kim, D.; Osuka, A. *Chem. Eur. J.* **2005**, *11*, 3389.
- (8) (a) Kim, D.; Osuka, A. *Acc. Chem. Res.* **2004**, *37*, 735. (b) Kim, D.; Osuka, A. *J. Phys. Chem.* **2003**, *107*, 8791. (c) Hwang, I.-W.; Aratani, N.; Osuka, A.; Kim, D. *Bull. Korean Chem. Soc.* **2005**, *26*, 1. (d) Aratani, N.; Cho, H. S.; Ahn, T. K.; Cho, S.; Kim, D.; Sumi, H.; Osuka, A. *J. Am. Chem. Soc.* **2003**, *125*, 9668.
- (9) (a) Ikeda, C.; Yoon, Z. S.; Park, M.; Inoue, H.; Kim, D.; Osuka, A. *J. Am. Chem. Soc.* **2005**, *127*, 534. (b) Ahn, T. K.; Kim, K. S.; Kim, D. Y.; Noh, S. B.; Aratani, N.; Ikeda, C.; Osuka, A.; Kim, D. *J. Am. Chem. Soc.* **2006**, *128*, 1700.
- (10) (a) Tsuda, A.; Furuta, H.; Osuka, A. *Angew. Chem., Int. Ed.* **2000**, *39*, 2549. (b) Tsuda, A.; Furuta, H.; Osuka, A. *J. Am. Chem. Soc.* **2001**, *123*, 10304. (c) Tsuda, A.; Osuka, A. *Science* **2001**, *293*, 79. (d) Cho, H. S.; Jeong, D. H.; Cho, S.; Kim, D.; Matsuzaki, Y.; Tanaka, K.; Tsuda, A.; Osuka, A. *J. Am. Chem. Soc.* **2002**, *124*, 14642.
- (11) (a) Bonifazi, D.; Scholl, M.; Song, F.; Echegoyen, L.; Accorsi, G.; Armaroli, N.; Dieterich, F. *Angew. Chem., Int. Ed.* **2003**, *42*, 4966. (b) Armaroli, N.; Accorsi, G.; Song, F.; Palkar, A.; Echegoyen, L.; Bonifazi, D.; Dieterich, F. *ChemPhysChem* **2005**, *6*, 732.
- (12) Sato, H.; Tashiro, K.; Shinmori, H.; Osuka, A.; Murata, Y.; Komatsu, K.; Aida, T. *J. Am. Chem. Soc.* **2005**, *127*, 13086.
- (13) Hwang, I.-W.; Ko, D. M.; Ahn, T. K.; Yoon, Z. S.; Kim, D.; Peng, X. B.; Aratani, N.; Osuka, A. *J. Phys. Chem. B* **2005**, *109*, 8643.
- (14) (a) Kasha, M. *Radiat. Res.* **1963**, *20*, 55. (b) Scholes, G. D.; Fleming, G. R. *J. Phys. Chem. B* **2000**, *104*, 1854.
- (15) (a) Yoon, Z. S.; Yoon, M.-C.; Kim, D. J. *Photochem. Photobiol. C: Photochem. Rev.* **2005**, *6*, 249. (b) Michl, T.; Thulstrup, E. W. *Spectroscopy with Polarized Light*; VCH: New York, 1986.

- (16) (a) Cho, H. S.; Rhee, H.; Song, J. K.; Min, C.-K.; Takase, M.; Aratani, N.; Cho, S.; Osuka, A.; Joo, T.; Kim, D. *J. Am. Chem. Soc.* **2000**, *125*, 5849. (b) Ha, J.-H.; Cho, H. S.; Song, J. K.; Kim, D.; Aratani, N.; Osuka, A. *ChemPhysChem* **2004**, *5*, 57.
- (17) Morandeira, A.; Vauthey, E.; Schuwey, A.; Gossauer, A. *J. Phys. Chem. A* **2004**, *108*, 5741.
- (18) Leegwater, J. A. *J. Phys. Chem.* **1996**, *100*, 14403.
- (19) Tanaka, H.; Nakagawa, T.; Kawai, T. *Surf. Sci.* **1996**, *364*, L575.

- (20) Selected examples of STM detection of porphyrin oligomers: (a) Bampos, N.; Woodburn, C. N.; Welland, M. E.; Sanders, J. K. M. *Angew. Chem. Int. Ed.* **1999**, *38*, 2780. (b) Kato, A.; Sugiura, K.; Miyasaka, H.; Tanaka, H.; Kawai, T.; Sugimoto, M.; Yamashita, M. *Chem. Lett.* **2004**, *33*, 578. (c) Shoji, O.; Tanaka, H.; Kawai, T.; Kobuke, Y. *J. Am. Chem. Soc.* **2005**, *127*, 8598.
- (21) Takagi, A.; Yanagawa, Y.; Tsuda, A.; Aratani, N.; Matsumoto, T.; Osuka, A.; Kawai, T. *Chem. Commun.* **2003**, 2986.